3 Diffraction from Periodic Structures

A direct imaging of atomic structures is nowadays possible using the high-resolution electron microscope, the field ion microscope, or the tunneling microscope. Nonetheless, when one wishes to determine an unknown structure, or make exact measurements of structural parameters, it is necessary to rely on diffraction experiments. The greater information content of such measurements lies in the fact that the diffraction process is optimally sensitive to the periodic nature of the solid's atomic structure. Direct imaging techniques, on the other hand, are ideal for investigating point defects, dislocations, and steps, and are also used to study surfaces and interfaces. In other words, they are particularly useful for studying features that represent a disruption of the periodicity.

For performing diffraction experiments one can make use of X-rays, electrons, neutrons and atoms. These various probes differ widely with respect to their elastic and inelastic interaction with the solid, and hence their areas of application are also different. Atoms whose particle waves have a suitable wavelength for diffraction experiments do not penetrate into the solid and are thus suitable for studying surfaces. The same applies, to a lesser extent, to electrons. Another important quantity which differs significantly for the various probes is the spatial extent of the scattering centers. Neutrons, for example, scatter from the nuclei of the solid's atoms, whereas X-ray photons and electrons are scattered by the much larger ($\sim 10^4$ times) electron shells. Despite this and other differences, which will be treated in more detail in Sect. 3.7, it is possible to describe the essential features of diffraction in terms of a single general theory. Such a theory is not able, of course, to include differences that arise from the polarization or spin polarization of the probes. The theory described in Sect. 3.1 below is quasi classical since the scattering itself is treated classically. The quantum mechanical aspects are treated purely by describing the probe particles as waves. For more detailed treatments including features specific to the various types of radiation, the reader is referred to [3.1–3.3].

3.1 General Theory of Diffraction

In our mathematical description of diffraction we will make the assumption of single scattering: the incoming wave induces the emission of spherical

H. Ibach, H. Lüth, *Solid-State Physics*, 4th ed.,
DOI 10.1007/978-3-540-93804-0_3,

waves at all points $\boldsymbol{r}$ of the target material. A fixed phase relationship is assumed between the primary wave and each of the emitted spherical waves (coherent scattering). Further scattering of the spherical waves, however, is neglected. This is also known as the "kinematic" approximation and corresponds to the first Born approximation of the quantum mechanical scattering theory. The approximation is valid for neutrons and X-rays, and within certain limits also for the scattering of high energy electrons. For highly perfect single crystals, it is possible to observe "nonkinematic" ("dynamical") effects in the scattering of X-rays.

For the derivation of the scattering amplitudes we make use of Fig. 3.1. Here Q is the location of the source of radiation, P is the position of the scattering center, and B the point of observation. As an example of a source we shall take the spherical light waves emitted in conjunction with an electronic transition in an atom. At sufficiently large distances from the source the spherical waves can be approximated as plane waves. The amplitude (or for X-rays more accurately the field strength vector) at position P and time t may thus be written

$$A_P = A_0 \, \mathrm{e}^{\mathrm{i}\boldsymbol{k}_0\cdot(\boldsymbol{R}+\boldsymbol{r})-\mathrm{i}\omega_0 t} \, . \tag{3.1}$$

If we follow this wave back to the source Q ($\boldsymbol{R} + \boldsymbol{r} = 0$), then its amplitude here as a function of time behaves as $\sim \exp(-\mathrm{i}\omega_0 \mathrm{t})$, i.e., it has a well-defined phase at all times. The reasoning, however, can only be applied to a *single* emission process. In real light sources photons are emitted with uncorrelated phases from many atoms (an exception to this is the laser). For other types of incident particle the phases are likewise uncorrelated. Thus, when we use expression (3.1), we must keep in mind that the result for the observed intensity arises by averaging over many individual diffraction events.

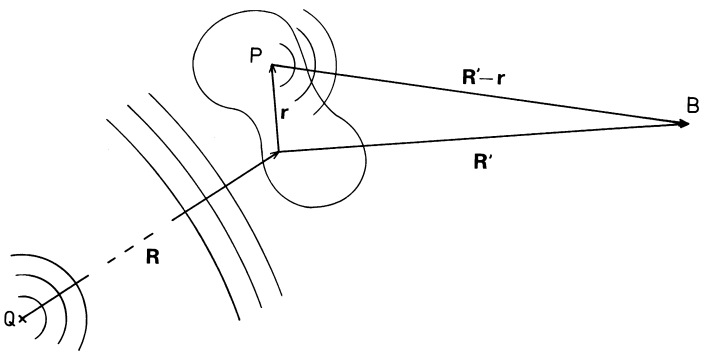

Fig. 3.1. Schematic representation of scattering indicating the parameters used in deriving the scattering kinematics. The source Q is assumed to be sufficiently far away from the target that the spherical waves reaching the target can be well approximated by plane waves. The same condition is assumed for the point of observation relative to the scattering centers

The relative phases of the wave at points P at time t are given by the position-dependent factor in (3.1). We now allow the primary wave to be scattered by the material. Every point P in the scattering material is caused by the primary wave to emit spherical waves, whose amplitude and phase relative to the incident (primary) wave are described by a complex scattering density $\varrho(\boldsymbol{r})$. The time dependence of these spherical waves is determined by the time dependence in (3.1) (forced oscillation). The spherical waves observed at B are therefore described by

$$A_B = A_P(\boldsymbol{r}, t)\, \varrho(\boldsymbol{r}) \frac{e^{ik|\boldsymbol{R}'-\boldsymbol{r}|}}{|\boldsymbol{R}'-\boldsymbol{r}|} . \tag{3.2}$$

For a fixed position P, the wave vector $\boldsymbol{k}$ is in the direction $\boldsymbol{R}'-\boldsymbol{r}$. Thus we can also write

$$A_B = A_P(\boldsymbol{r}, t)\, \varrho(\boldsymbol{r}) \frac{e^{i\boldsymbol{k}\cdot(\boldsymbol{R}'-\boldsymbol{r})}}{|\boldsymbol{R}'-\boldsymbol{r}|} . \tag{3.3}$$

At large distances from the scattering center A_B is then given by

$$A_B = A_P(\boldsymbol{r}, t)\, \varrho(\boldsymbol{r}) \frac{1}{R'} e^{i\boldsymbol{k}\cdot(\boldsymbol{R}'-\boldsymbol{r})} \tag{3.4}$$

where $\boldsymbol{k}$ now has the same direction for *all* positions P in the target material.

Inserting (3.1) into (3.4) we obtain

$$A_B = \frac{A_0}{R'} e^{i(\boldsymbol{k}_0\cdot\boldsymbol{R}+\boldsymbol{k}\cdot\boldsymbol{R}')} e^{-i\omega_0 t}\, \varrho(\boldsymbol{r})\, e^{i(\boldsymbol{k}_0-\boldsymbol{k})\cdot\boldsymbol{r}} . \tag{3.5}$$

The total scattering amplitude is given by integration over the entire scattering region:

$$A_B(t) \propto e^{-i\omega_0 t} \int \varrho(\boldsymbol{r})\, e^{i(\boldsymbol{k}_0-\boldsymbol{k})\cdot\boldsymbol{r}} d\boldsymbol{r} . \tag{3.6}$$

For scattering from a rigid lattice, $\varrho(\boldsymbol{r})$ is time independent and the time dependence of A_B only contains the frequency ω_0. In the quantum mechanical picture this corresponds to energy conservation. We thus have elastic scattering. This form of scattering is important for structural analyses. If instead we allow the scattering density $\varrho(\boldsymbol{r})$ to vary with time, then we also obtain scattered waves with $\omega \neq \omega_0$. This inelastic scattering will be dealt with in Sect. 4.4.

In diffraction experiments for structure determination, it is not the amplitude but the intensity of the scattered waves that is measured:

$$I(\boldsymbol{K}) \propto |A_B|^2 \propto \left|\int \varrho(\boldsymbol{r})\, e^{-i\boldsymbol{K}\cdot\boldsymbol{r}}\, d\boldsymbol{r}\right|^2 . \tag{3.7}$$

In this equation we have introduced the scattering vector $\boldsymbol{K} = \boldsymbol{k}-\boldsymbol{k}_0$.

We see that the intensity is the absolute square of the Fourier transform of the scattering density $\varrho(\boldsymbol{r})$ with respect to the scattering vector $\boldsymbol{K}$. From this we establish an important fact: The smaller the structures to be resolved in the diffraction measurement, the larger is the required value of $\boldsymbol{K}$, and thus

also of the $\boldsymbol{k}$-vector of the incident radiation. In studies of the atomic structures of solids the wavelengths should thus roughly correspond to the lattice constants. For such waves it is impossible to measure their amplitude as a function of position and time – only the intensity can be measured. This leads to considerable complications in structural analysis. If it were actually possible to measure the amplitude instead of the intensity, then one could make use of inverse Fourier transformation to obtain the spatial distribution of the scattering density directly from the diffraction pattern. However, since in reality one can only observe the intensities, the information about the phases is lost and the scattering density cannot be calculated directly. To determine a particular structure it is therefore necessary to do the calculation in reverse: One chooses a feasible model structure, calculates the diffraction pattern that it would produce, and then compares this with the experimentally observed diffraction pattern. The structural parameters of the model are varied until optimal agreement with experiment is found.

The analysis of unknown structures is facilitated by invoking the so-called Patterson function, which is the Fourier transform of the intensity. In order to elucidate the meaning of the Patterson function we rewrite (3.7) for the intensity

$$I(\boldsymbol{K}) \propto \int \varrho(\boldsymbol{r})\, \mathrm{e}^{-\mathrm{i}\boldsymbol{K}\cdot\boldsymbol{r}}\, d\boldsymbol{r} \int \varrho(\boldsymbol{r}')\, \mathrm{e}^{\mathrm{i}\boldsymbol{K}\cdot\boldsymbol{r}'} d\boldsymbol{r}' \,. \tag{3.8}$$

Since both integrals extend over the entire space the variable $\boldsymbol{r}'$ in the second integral can be replaced by $\boldsymbol{r} + \boldsymbol{r}'$. Hence, one obtains

$$I(\boldsymbol{K}) \propto \int \mathrm{e}^{\mathrm{i}\boldsymbol{K}\cdot\boldsymbol{r}'}\, d\boldsymbol{r}' \int \varrho(\boldsymbol{r}) \varrho(\boldsymbol{r}' + \boldsymbol{r})\, d\boldsymbol{r} \,. \tag{3.9}$$

The auto-correlation function of the scattering density

$$P(\boldsymbol{r}') = \int \varrho(\boldsymbol{r})\, \varrho(\boldsymbol{r}' + \boldsymbol{r}) d\boldsymbol{r} \tag{3.10}$$

is the Patterson function. The function has its peaks where $\boldsymbol{r}'$ corresponds to a vector between two atoms of the crystal structure. A peak is particularly strong if the vector connects two atoms with a large scattering cross section. The interatomic distances in an unknown structure are therefore easily obtained by inspection of the Patterson function.

Scattering from disordered systems, i.e. liquids and amorphous solids is most suitably described with the help of the Patterson function $P(\boldsymbol{r}')$. We decompose the scattering density $\varrho(\boldsymbol{r})$ into contributions from individual atoms. For simplicity we assume that the material is made up of a single type of atoms. The scattering density centered at the position $\boldsymbol{r}_i$ is denoted as $\varrho_{\mathrm{at}}(\boldsymbol{r}-\boldsymbol{r}_i)$.

$$\varrho(\boldsymbol{r}) = \sum_i \varrho_{\mathrm{at}}(\boldsymbol{r} - \boldsymbol{r}_i) \,. \tag{3.11}$$

The Patterson-function $P(\boldsymbol{r}')$ can be split into two contributions: one describing the correlation of one atom with itself and the other one describing the correlation of an atom with all other atoms.

$$P(\boldsymbol{r}') = \sum_{i,j} \int \varrho_{\mathrm{at}}(\boldsymbol{r} - \boldsymbol{r}_i)\varrho_{\mathrm{at}}(\boldsymbol{r} - \boldsymbol{r}_j + \boldsymbol{r}')d\boldsymbol{r}$$
$$= \sum_{i} \int \varrho_{\mathrm{at}}(\boldsymbol{r} - \boldsymbol{r}_i)\varrho_{\mathrm{at}}(\boldsymbol{r} - \boldsymbol{r}_i + \boldsymbol{r}')d\boldsymbol{r} + \sum_{i} \int \varrho_{\mathrm{at}}(\boldsymbol{r} - \boldsymbol{r}_i)$$
$$\times \sum_{j \neq i} \varrho_{\mathrm{at}}(\boldsymbol{r} - \boldsymbol{r}_j + \boldsymbol{r}')d\boldsymbol{r} \,. \tag{3.12}$$

The second term in (3.12) contains the information on the structure. We assume now that the scattering density is localized at the centers of the atoms. This assumption is particularly well fulfilled for neutron scattering (see also Sect. 3.7 and I.3). In that case, the first integral in (3.12) contributes only at $\boldsymbol{r}' = 0$. The integral can therefore be replaced by $f^2\delta_{0,r'}$ where $\delta_{0,r'}$ denotes the Kronecker symbol and f the "atom factor", which is a measure of the magnitude of the scattering amplitude of an atom. The sum over all (identical) atoms i in the first term can be replaced by a multiplication with the number of atoms N. The second integral in (3.12) vanishes for $\boldsymbol{r}' = 0$ since the probability to have a second atom j at the position of any other atom i is zero. We assume the system to be disordered, but homogeneous on a coarse scale. Because of the disorder, the mean scattering density around each atom is identical and independent of angle. Thus, the mean value of the sum

$$\bar{\varrho}(r) = \left\langle \sum_{j \neq i} \varrho_{\mathrm{at}}(\boldsymbol{r} - \boldsymbol{r}_j) \right\rangle$$

depends only on the distance r from the atom whose environment is being considered.

The Patterson function is then

$$P(r') = Nf^2\delta_{0,r'} + N\int \varrho(r)\overline{\varrho}(r + r')d\boldsymbol{r} \,. \tag{3.13}$$

It is useful to introduce a function $g(r')$ that is a measure of the pair correlation of atoms, independent of their scattering amplitude and density. The limiting value of $g(r')$ for $r' \to \infty$ is one. For large distances away from any particular atom considered the scattering density is $\lim_{r' \to \infty} \overline{\varrho}(r + r') = Nf/V$ with V the volume. We therefore define the function $g(r')$ by

$$\frac{N}{V} f^2 g(r') = \int \varrho(r)\,\overline{\varrho}(r + r')\,d\boldsymbol{r} \,. \tag{3.14}$$

After inserting (3.14) and (3.13) in (3.9) one obtains for the scattering intensity $I(\boldsymbol{K})$

$$I(\boldsymbol{K}) \propto S(\boldsymbol{K}) = 1 + \frac{N}{V}\int g(r)\, \mathrm{e}^{\mathrm{i}\boldsymbol{K}\cdot\boldsymbol{r}} d\boldsymbol{r} \,. \tag{3.15}$$

$S(\boldsymbol{K})$ is known as the structure factor. The pair correlation function $g(r)$ can be calculated from the Fourier transform of $S(\boldsymbol{K}) - 1$. Here, however, one

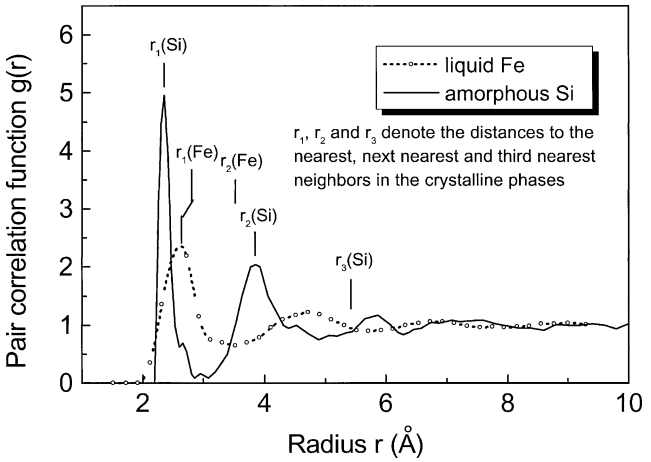

Fig. 3.2. Pair correlation function for amorphous silicon and liquid iron at a temperature of $T = 1833\,\mathrm{K}$ [3.4, 3.5]. The distances of the nearest, next-nearest, and third nearest-neighbors for crystalline silicon are marked as r_1(Si), r_2(Si) and r_3(Si), the corresponding distances for crystalline iron (fcc structure) as r_1(Fe) and r_2(Fe)

encounters a technical difficulty: The contribution to $g(r)$ that arises from the homogeneous part of the scattering density at large r leads to a forward scattering at $\boldsymbol{K} = 0$. This contribution cannot be separated from the primary beam. One therefore extracts a function $h(r) = g(r) - 1$ from the experimental data that does not include the forward scattering. The function $h(r)$ is therefore the Fourier transform of the structure factor without the forward-scattering contribution (see Problem 3.7). Figure 3.2 shows two examples for the pair correlation function $g(r)$. The dashed and full lines represent $g(r)$ for liquid iron and amorphous silicon, respectively. The first peak corresponds to the distance of nearest-neighbors. The sharpness of the peak indicates that the distance to the nearest-neighbor is well defined even for structurally disordered systems. The mean distances of further neighbors are likewise discernible. Here, we encounter a characteristic difference between the amorphous state and the liquid state of matter. In the amorphous state, the distance to the next nearest-neighbor is nearly the same as in the crystalline state. The lower density of the amorphous state is reflected only in the distance to the third nearest-neighbor. In liquids, the second peak is approximately at twice the distance of the nearest-neighbor peak, hence at a significantly larger distance than, e.g., in a close-packed solid. This larger distance of second nearest-neighbors is an essential feature of the liquid state. Only with a larger distance of second nearest-neighbors can a liquid state be realized, as is easily demonstrated in a model in which the atoms are represented as hard spheres (see also Problem 3.7b).

3.2 Periodic Structures and the Reciprocal Lattice

For periodic structures, $\varrho(\boldsymbol{r})$ can be expanded in a Fourier series. We first consider a one-dimensional example in which $\varrho(x)$ repeats with period a

$$\varrho(x) = \varrho(x + n\,a) \quad n = 0, \pm 1, \pm 2, \ldots . \tag{3.16}$$

The corresponding Fourier series then reads

$$\varrho(x) = \sum_n \varrho_n \, \mathrm{e}^{\mathrm{i}(n\,2\pi/a)\,x} . \tag{3.17}$$

It is readily seen that a displacement by an arbitrary lattice vector $x_m = m\,a$ leads to an identical $\varrho(x)$, hence satisfying the required translational invariance. The extension to three dimensions is straightforward and yields

$$\varrho(\boldsymbol{r}) = \sum_{\boldsymbol{G}} \varrho_{\boldsymbol{G}} \, \mathrm{e}^{\mathrm{i}\,\boldsymbol{G}\cdot\boldsymbol{r}} . \tag{3.18}$$

The vector $\boldsymbol{G}$ must fulfill certain conditions in order to preserve the translational invariance of ϱ with respect to all lattice vectors

$$\boldsymbol{r}_n = n_1\,\boldsymbol{a}_1 + n_2\,\boldsymbol{a}_2 + n_3\,\boldsymbol{a}_3 . \tag{3.19}$$

The conditions are expressed by

$$\boldsymbol{G}\cdot\boldsymbol{r}_n = 2\pi\,m \tag{3.20}$$

where m is an integer for all values of n_1, n_2, n_3. We now decompose $\boldsymbol{G}$ in terms of three as yet undetermined basis vectors $\boldsymbol{g}_i$,

$$\boldsymbol{G} = h\,\boldsymbol{g}_1 + k\,\boldsymbol{g}_2 + l\,\boldsymbol{g}_3 \tag{3.21}$$

with integer h, k, l. The condition (3.20) now implies for the example of $n_2 = n_3 = 0$

$$(h\,\boldsymbol{g}_1 + k\,\boldsymbol{g}_2 + l\,\boldsymbol{g}_3)\,n_1\,\boldsymbol{a}_1 = 2\pi\,m . \tag{3.22}$$

For an arbitrary choice of n_1 this can only be satisfied if

$$\boldsymbol{g}_1\cdot\boldsymbol{a}_1 = 2\pi \quad \text{and} \quad \boldsymbol{g}_2\cdot\boldsymbol{a}_1 = \boldsymbol{g}_3\cdot\boldsymbol{a}_1 = 0 . \tag{3.23}$$

Expressed in general terms this requirement becomes

$$\boldsymbol{g}_i\cdot\boldsymbol{a}_j = 2\pi\,\delta_{ij} . \tag{3.24}$$

The basis set $\boldsymbol{g}_1, \boldsymbol{g}_2, \boldsymbol{g}_3$ that we have thus defined spans the so-called reciprocal lattice. For every real lattice there is a corresponding and unambiguously defined reciprocal lattice. Its lattice points are denoted by the numbers h, k, l. The rules for constructing this lattice are given directly by (3.24): the reciprocal lattice vector $\boldsymbol{g}_1$ lies perpendicular to the plane containing $\boldsymbol{a}_2$ and $\boldsymbol{a}_3$ and its length is $2\pi/a_1$ [$\cos \sphericalangle(\boldsymbol{g}_1, \boldsymbol{a}_1)$]. Figure 3.3 shows a planar oblique lattice and its corresponding reciprocal lattice. It should be noted however that, although the reciprocal lattice is drawn here in real space, its dimensions are actually m^{-1}.

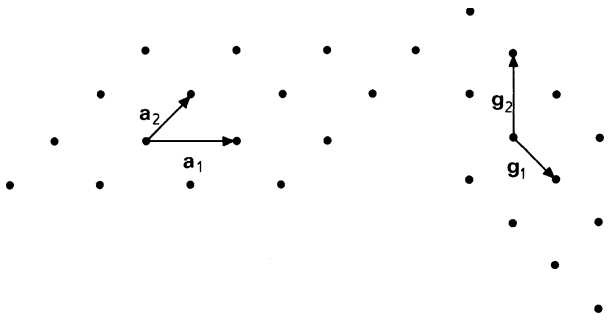

Fig. 3.3. A plane oblique lattice and its corresponding reciprocal lattice. The vectors $\boldsymbol{g}_1$ and $\boldsymbol{g}_2$ lie perpendicular to $\boldsymbol{a}_2$ and $\boldsymbol{a}_1$ respectively

A useful expression for the basis vectors of the reciprocal lattice is the following

$$\boldsymbol{g}_1 = 2\pi \frac{\boldsymbol{a}_2 \times \boldsymbol{a}_3}{\boldsymbol{a}_1 \cdot (\boldsymbol{a}_2 \times \boldsymbol{a}_3)} \quad \text{and cyclic permutations.} \tag{3.25}$$

It is easy to show that (3.25) satisfies the condition (3.24).

It follows from the one-to-one correspondence of the lattice and its reciprocal lattice that every symmetry property of the lattice is also a symmetry property of the reciprocal lattice. The reciprocal lattice therefore belongs to the same point group as the real-space lattice.

3.3 The Scattering Conditions for Periodic Structures

We now proceed to insert the Fourier expansion of $\varrho(\boldsymbol{r})$ into the equation (3.7) for the scattering intensity. With the notation $\boldsymbol{K} = \boldsymbol{k} - \boldsymbol{k}_0$ we obtain

$$I(\boldsymbol{K}) \propto \frac{|A_0|^2}{R'^2} \left| \sum_{\boldsymbol{G}} \varrho_{\boldsymbol{G}} \int \mathrm{e}^{\mathrm{i}(\boldsymbol{G}-\boldsymbol{K})\cdot\boldsymbol{r}}\, d\boldsymbol{r} \right|^2 . \tag{3.26}$$

If the crystal consists of many identical unit cells, the only significant contributions to the integral in (3.26) arise when $\boldsymbol{G} = \boldsymbol{K}$. Expressed in its components, this integral would be, for an infinite volume, a representation of the respective δ-functions. Its value is then equal to the scattering volume V

$$\int \mathrm{e}^{\mathrm{i}(\boldsymbol{G}-\boldsymbol{K})\cdot\boldsymbol{r}}\, d\boldsymbol{r} = \begin{cases} V & \text{für} \quad \boldsymbol{G} = \boldsymbol{K} \\ \sim 0 & \text{otherwise} \end{cases} . \tag{3.27}$$

Scattering from lattices thus leads to diffracted beams when the difference between the $\boldsymbol{k}$ vectors of the incident and scattered waves is equal to a reciprocal lattice vector $\boldsymbol{G}$. This condition is named the "Laue condition" after Max von Laue. The measured intensity is

$$I(\boldsymbol{K}=\boldsymbol{G}) \propto \frac{|A_0|^2}{R'^2} |\varrho_{\boldsymbol{G}}|^2 V^2 . \tag{3.28}$$

The apparent proportionality to V^2 needs further comment. An exact analysis of the integral shows in fact that the width of the intensity distribution around a diffraction beam maximum decreases as V^{-1}. Thus, as expected, the total intensity is proportional to the scattering volume.

The vector $\boldsymbol{G}$ is unambiguously defined by its coordinates h,k,l with respect to the basis vectors $\boldsymbol{g}_i$ of the reciprocal lattice. Thus the indices h,k,l can also be used to label the diffraction beams. Negative values of h,k,l are denoted by $\bar{h},\bar{k},\bar{l}$

$$I_{hkl} \propto |\varrho_{hkl}|^2 . \tag{3.29}$$

If no absorption of radiation takes place in the target material, $\varrho(\boldsymbol{r})$ is a real function and on account of (3.18) we then have

$$\varrho_{hkl} = \varrho^*_{\bar{h}\bar{k}\bar{l}} . \tag{3.30}$$

This means that the intensities obey

$$I_{hkl} = I_{\bar{h}\bar{k}\bar{l}} \quad \text{(Friedel's rule)} . \tag{3.31}$$

The above rule has an interesting consequence. The X-ray pattern always displays a center of inversion, even when none is present in the structure itself. For structures containing a polar axis, the orientation of this axis cannot be determined from the X-ray diffraction pattern. An exception to this statement is found when one works in a region of strong absorption, i.e., when the above condition of a real scattering density does not hold.

We now devote some more attention to the interpretation of the Laue condition

$$\boldsymbol{K} = \boldsymbol{G} . \tag{3.32}$$

This condition is of fundamental importance for all diffraction phenomena involving periodic structures, regardless of the type of radiation employed. It can be represented pictorially by means of the Ewald construction (Fig. 3.4). One selects an arbitrary reciprocal lattice point as the origin and draws the vector $\boldsymbol{k}_0$ to point towards the origin. Since we are assuming elastic scattering we have $k = k_0 = 2\pi/\lambda$ where λ is the wavelength of the radiation. All points on the sphere of radius $k = k_0$ centered around the starting point of the vector $\boldsymbol{k}_0$ describe the end points of a vector $\boldsymbol{K} = \boldsymbol{k} - \boldsymbol{k}_0$. The condition $\boldsymbol{G} = \boldsymbol{K}$ is satisfied whenever the surface of the sphere coincides with points of the reciprocal lattice. At these points diffraction beams are produced and they are labeled with the indices (hkl) corresponding to the relevant reciprocal lattice point.

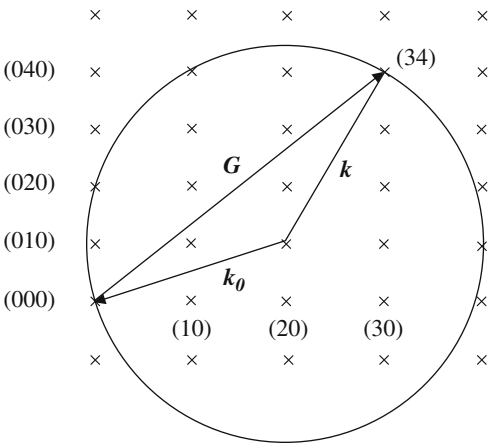

Fig. 3.4. The Ewald sphere of the reciprocal lattice illustrating the Laue condition $\boldsymbol{k} - \boldsymbol{k}_0 = \boldsymbol{G}$. Diffraction beams are produced whenever a reciprocal lattice point coincides with the surface of the sphere. For arbitrary values of the magnitude and direction of $\boldsymbol{k}_0$ this will generally not be the case. In order to observe diffraction one must either use a continuum of incident wavelengths or vary the orientation of the crystal

3.4 The Bragg Interpretation of the Laue Condition

Any three lattice points that do not lie on a straight line can be seen (Fig. 3.5) to define a so-called lattice plane. Such lattice planes may be labeled in a manner that leads to a particularly simple interpretation of the diffraction from the lattice. We assume that the lattice plane intersects the coordinate axes at values

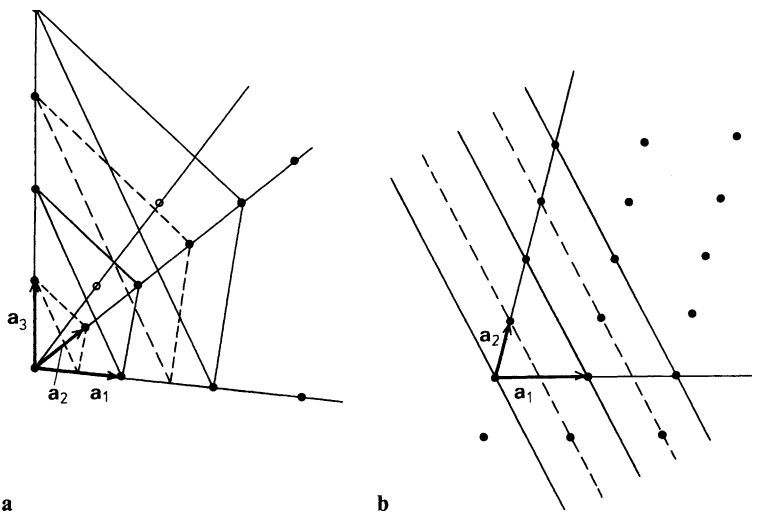

Fig. 3.5 a, b. Sets of crystal lattice planes. The planes illustrated here have the values $m = 1$, $n = 2$, $o = 2$. The corresponding Miller indices are derived for the triplet $(1/m, 1/n, 1/o)$ by multiplying this by an integer $p = 2$ to give $(hkl) = (211)$. Between the planes with indices m, n, o there lie additional planes (*dotted lines*). These contain the same density of atoms as can be seen from Fig. 3.4 b, and are thus completely equivalent to the original planes. The perpendicular separation of equivalent lattice plane is exactly a factor of p smaller than the separation of the original planes (*full lines*) constructed from the positions of atoms lying on the coordinate axes

m,n,o, where each of these numbers denotes an integer multiple of the corresponding basis vector. One then takes the reciprocal values $h' = 1/m, k' = 1/n, l' = 1/o$ and multiplies h', k', l' by an integer p so as to obtain a triplet of coprime integers (h,k,l). The numbers h,k,l are known as the Miller indices of the lattice plane (hkl). Parallel to the planes that intersect each axis at a lattice point (full lines in Fig. 3.5) one can also draw other equivalent lattice planes. The number of these planes is such that every lattice point on each of the three axes lies in one of these lattice planes. This is a consequence of the required translational symmetry (Fig. 3.5 b). The total number of equivalent lattice planes is now exactly p times as many as the number of original planes (full lines). The reciprocal values of the axis intersection of these planes (dotted and full lines in Fig. 3.5) directly supply the required index triplet (hkl) of coprime integers.

We now prove an important relation: The reciprocal lattice vector $\boldsymbol{G}$ with components (hkl) lies perpendicular to the lattice plane with the same indices (hkl). The length of the vector $\boldsymbol{G}_{hkl}$ is equal to 2π times the reciprocal distance between neighboring (hkl) planes.

We begin by proving the first part of this statement. The vectors

$$\frac{\boldsymbol{a}_1}{h'} - \frac{\boldsymbol{a}_2}{k'} \quad \text{and} \quad \frac{\boldsymbol{a}_3}{l'} - \frac{\boldsymbol{a}_2}{k'}$$

span the lattice plane. Their vector product

$$\left(\frac{\boldsymbol{a}_1}{h'} - \frac{\boldsymbol{a}_2}{k'}\right) \times \left(\frac{\boldsymbol{a}_3}{l'} - \frac{\boldsymbol{a}_2}{k'}\right) = -\frac{1}{h'k'}(\boldsymbol{a}_1 \times \boldsymbol{a}_2) - \frac{1}{k'l'}(\boldsymbol{a}_2 \times \boldsymbol{a}_3) - \frac{1}{h'l'}(\boldsymbol{a}_3 \times \boldsymbol{a}_1) \tag{3.33}$$

is normal to the plane (hkl). On multiplying this vector by $-2\pi h'k'l'/[\boldsymbol{a}_1 \cdot (\boldsymbol{a}_2 \times \boldsymbol{a}_3)]$ one obtains

$$2\pi\left(h' \frac{\boldsymbol{a}_2 \times \boldsymbol{a}_3}{\boldsymbol{a}_1 \cdot (\boldsymbol{a}_2 \times \boldsymbol{a}_3)} + k' \frac{\boldsymbol{a}_3 \times \boldsymbol{a}_1}{\boldsymbol{a}_1 \cdot (\boldsymbol{a}_2 \times \boldsymbol{a}_3)} + l' \frac{\boldsymbol{a}_1 \times \boldsymbol{a}_2}{\boldsymbol{a}_1 \cdot (\boldsymbol{a}_2 \times \boldsymbol{a}_3)}\right). \tag{3.34}$$

This however, apart from the numerical factor p, is equal to $\boldsymbol{G}_{hkl}$ [see (3.21) and (3.25)]. Thus we have demonstrated that $\boldsymbol{G}_{hkl}$ lies perpendicular to the plane (hkl).

We now show that the separation of the planes, d_{hkl}, is equal to $2\pi/G_{hkl}$. The perpendicular distance of the lattice plane (hkl) from the origin of the basis $\boldsymbol{a}_1, \boldsymbol{a}_2, \boldsymbol{a}_3$ is

$$d'_{hkl} = \frac{a_1}{h'} \cos \sphericalangle(\boldsymbol{a}_1, \boldsymbol{G}_{hkl}) \tag{3.35}$$

$$= \frac{a_1}{h'} \frac{\boldsymbol{a}_1 \cdot \boldsymbol{G}_{hkl}}{a_1 G_{hkl}} = \frac{2\pi}{G_{hkl}} \frac{h}{h'} = \frac{2\pi}{G_{hkl}} p\,. \tag{3.36}$$

The distance to the *nearest* lattice plane is therefore $d_{hkl} = d'_{hkl}/p = 2\pi/G_{hkl}$.

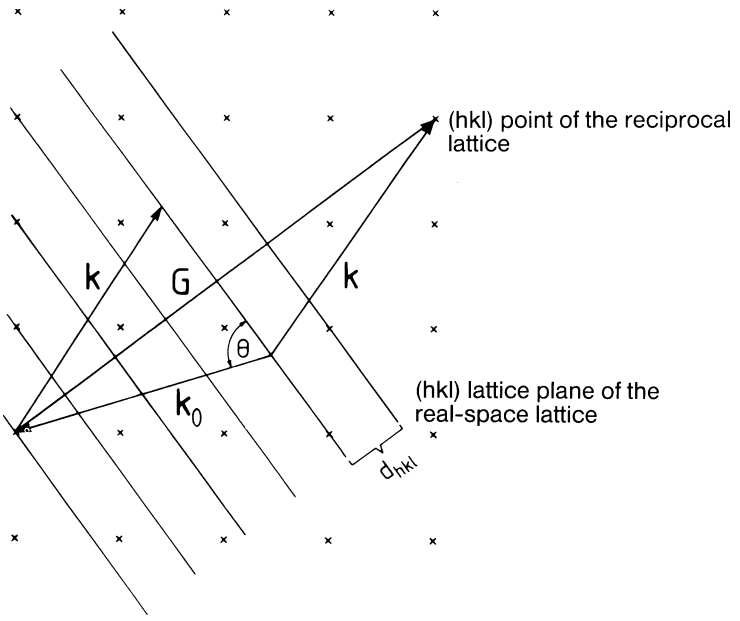

Fig. 3.6. The Bragg interpretation of the scattering condition. Since the vector $\boldsymbol{G}_{hkl}$ lies perpendicular to the lattice planes (hkl) in real space, the scattering appears to be a mirror reflection from these planes. It should be noted that real space and reciprocal space are shown here superposed

With the help of the lattice planes it is possible to obtain an intuitively clear interpretation of the scattering conditions. We take the modulus of the equation $\boldsymbol{G} = \boldsymbol{K}$:

$$G_{hkl} = \frac{2\pi}{d_{hkl}} = 2k_0 \sin \Theta \quad \text{(Fig. 3.6)} \tag{3.37}$$

and thereby obtain the Bragg equation

$$\lambda = 2 d_{hkl} \sin \Theta . \tag{3.38}$$

This equation implies that the waves behave as if they were reflected from the lattice planes (hkl) (Fig. 3.6). It is from this interpretation that the expression "Bragg reflection" stems. The scattering condition then amounts to the requirement that the path difference between waves reflected from successive lattice planes should be an integer multiple of the wavelength of the radiation, such as is needed to produce constructive interference (Fig. 3.7).

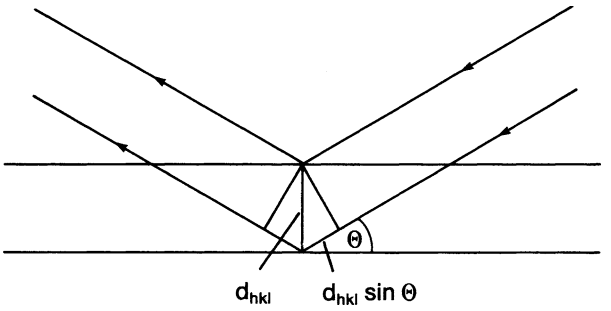

Fig. 3.7. Derivation of the Bragg condition. The path difference of the two reflected waves is $2d_{hkl} \sin \Theta$

3.5 Brillouin Zones

The condition for the occurrence of a Bragg reflection was $\boldsymbol{k} - \boldsymbol{k}_0 = \boldsymbol{G}_{hkl}$. The end points of all vector pairs $\boldsymbol{k}, \boldsymbol{k}_0$ that satisfy this condition lie on the perpendicular bisector of $\boldsymbol{G}_{hkl}$ (Fig. 3.4). The smallest polyhedron centered at the origin and enclosed by perpendicular bisectors of reciprocal lattice vectors is called the Brillouin zone (also first Brillouin zone). The construction of the Brillouin zone is best demonstrated for the case of an oblique planar lattice (Fig. 3.8).

The Brillouin zones for a few simple three-dimensional lattices are shown in Fig. 3.9. The symbols denoting points in the Brillouin zone originate from group theory and characterize the symmetry. Like the reciprocal lattice, the Brillouin zone also possesses the same point symmetry as the respective lattice type.

The points on the zone boundary are special because every wave with a $\boldsymbol{k}$-vector extending from the origin to the zone boundary gives rise to a Bragg-reflected wave. In the case of weak scattering and small crystals this wave has only a small intensity. For large single crystals however, the intensities of the primary and Bragg-reflected waves may be equal. These interfere to produce a standing wave field. The position of the nodes and antinodes is determined by the relative phases of the two waves and can be varied by changing the angle of incidence of the primary beam. This effect

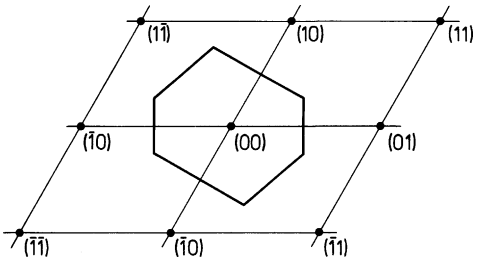

Fig. 3.8. Construction of the first Brillouin zone for a plane oblique lattice. Further zones can be constructed from the perpendicular bisectors of larger reciprocal lattice vectors

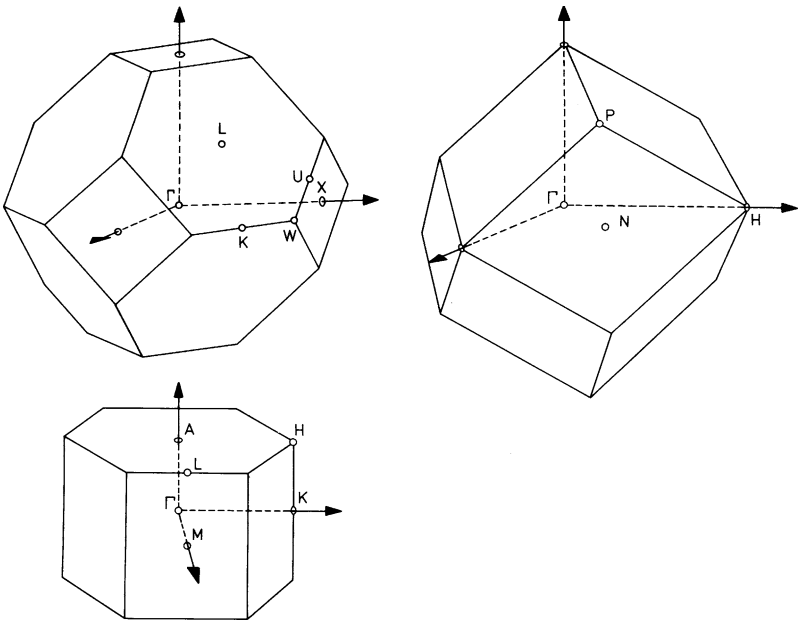

Fig. 3.9. The Brillouin zones of the face-centered cubic, body-centered cubic and hexagonal lattices. Points of high symmetry are denoted by Γ, L, X etc. The surfaces enclosing the Brillouin zones are parts of the planes that perpendicularly bisect the smallest reciprocal lattice vectors. The polyhedra that are produced by these rules of construction can be drawn about every point of the reciprocal lattice. They then fill the entire reciprocal space. The cell produced by the equivalent construction in real space is known as the Wigner-Seitz cell. It can be used to describe the volume that one may assign to each point of the real crystal lattice

can be used, for example, to determine the position of impurity atoms in a lattice via the observation of their X-ray fluorescence. The production of two waves of equal intensity and a fixed phase relation can also be used to construct an X-ray interferometer with which individual lattice defects can be imaged (Panel II).

For the case of electrons in a periodic solid, the production of Bragg-reflected waves and their significance for the electron bands of the solid will be discussed at greater length in Chap. 7.

3.6 The Structure Factor

The scattering condition (3.27) predicts only the positions at which diffraction beams appear. To obtain their intensity from (3.26) we first need to calculate the Fourier coefficients ϱ_{hkl} of the scattering density

$$\varrho_{hkl} = \frac{1}{V_c} \int_{\text{cell}} \varrho\,(\boldsymbol{r}) \mathrm{e}^{-\mathrm{i}\boldsymbol{G}\cdot\boldsymbol{r}}\, d\boldsymbol{r}\,. \tag{3.39}$$

In this the integral extends over the unit cell. By substituting the Fourier expansion (3.18) of $\varrho(\boldsymbol{r})$ one can convince oneself of the validity of this equation. The scattering of X-rays is due to the electrons of the atoms. Except in the case of light elements, the majority of the solid's electrons (the core electrons) are concentrated in a small region around the atoms. Scattering from the valence electrons, which extend into the region between the atoms, can be neglected in comparison. The integral over the scattering density $\varrho(\boldsymbol{r})$ can therefore be divided into single integrals over the individual atoms: these must then be added together with the appropriate phases. For this it is convenient to divide the position vector $\boldsymbol{r}$ into a vector $\boldsymbol{r_n}$ that gives the position of the origin of the nth unit cell, a vector $\boldsymbol{r}_\alpha$ defining the position of each atom within the unit cell, and a new position vector $\boldsymbol{r}'$ which points away from the center of each atom: $\boldsymbol{r} = \boldsymbol{r_n} + \boldsymbol{r}_\alpha + \boldsymbol{r}'$ (Fig. 3.10). With this notation, the Fourier coefficients of the scattering density can be expressed as

$$\varrho_{hkl} = \frac{1}{V_c} \sum_{\alpha} \mathrm{e}^{-\mathrm{i}\boldsymbol{G}\cdot\boldsymbol{r}_\alpha} \int \varrho_\alpha\,(\boldsymbol{r}')\, \mathrm{e}^{-\mathrm{i}\boldsymbol{G}\cdot\boldsymbol{r}'}\, d\boldsymbol{r}'\,. \tag{3.40}$$

The integral now extends only over the volume of a single atom. It is evident that it describes the interference of the spherical waves emanating from different points within the atom. This integral is known as the atomic scattering factor.

Since the scattering density is essentially spherically symmetric about each atom, the integral can be further evaluated by introducing spherical polar coordinates

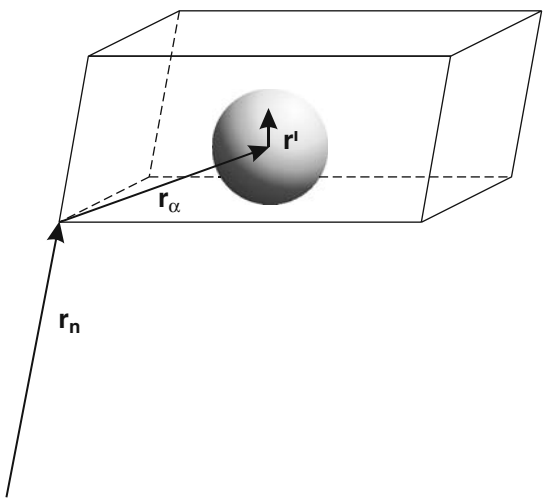

Fig. 3.10. Definition of the vectors r_n, r_α and r'. The vector r_n points to the origin of the nth unit cell, which is described by the triplet $n = n_1,n_2,n_3$, r_α points to the center of an atom within the cell, and r' from the center to a point within the atom

$$f_\alpha = \int \varrho_\alpha(\boldsymbol{r}')\mathrm{e}^{-\mathrm{i}\,\boldsymbol{G}\cdot\boldsymbol{r}'}d\boldsymbol{r}' = -\int \varrho_\alpha(\boldsymbol{r}')\,\mathrm{e}^{-\mathrm{i}Gr'\cos\vartheta}\,r'^2 dr'\,d(\cos\vartheta)\,d\varphi\,. \tag{3.41}$$

Here ϑ is the polar angle between $\boldsymbol{G}$ and $\boldsymbol{r}'$. On integrating over ϑ and φ one obtains

$$f_\alpha = 4\pi \int \varrho_\alpha(r')\,r'^2\,\frac{\sin\,Gr'}{Gr'}\,dr'\,. \tag{3.42}$$

If we denote the angle between $\boldsymbol{k}$ and $\boldsymbol{k}_0$ as the scattering angle 2Θ (forward scattering: $\Theta = 0$) then on account of the relation

$$G = 2k_0 \sin\,\Theta\,, \tag{3.43}$$

it follows that

$$f_\alpha = 4\pi \int \varrho_\alpha(r')\,r'^2\,\frac{\sin\,[4\pi r'(\sin\Theta/\lambda)]}{4\pi r'(\sin\Theta/\lambda)}\,dr'\,. \tag{3.44}$$

Thus the atomic scattering factor is a function $f(\sin\Theta/\lambda)$ which has its maximum value for forward scattering. For $\Theta = 0$ we have $f = 4\pi\int\varrho(r')r'^2dr'$, i.e. it is equal to the integral of the scattering density over the atomic volume. For X-ray scattering this is proportional to Z, the total number of electrons per atom.

The summation over α in (3.40) leads to the so-called structure factor S_{hkl}. This describes the interference between waves scattered from the different atoms within the unit cell,

$$S_{hkl} = \sum_\alpha f_\alpha\,\mathrm{e}^{-\mathrm{i}\,\boldsymbol{G}_{hkl}\cdot\boldsymbol{r}_\alpha}\,. \tag{3.45}$$

For primitive lattices, i.e., those with only one atom per unit cell, $S = f$. Other special cases arise for centered lattices. To show this we describe the vector $\boldsymbol{r}_\alpha$ in units of the basis vectors of the lattice

$$\boldsymbol{r}_\alpha = u_\alpha\,\boldsymbol{a}_1 + v_\alpha\,\boldsymbol{a}_2 + w_\alpha\,\boldsymbol{a}_3\,. \tag{3.46}$$

Since $\boldsymbol{r}_\alpha$ is within the unit cell, we have $u, v, w < 1$. Using the definition of the reciprocal lattice vectors (3.24) the structure factor may be written

$$S_{hkl} = \sum_\alpha f_\alpha\,\mathrm{e}^{-2\pi\mathrm{i}\,(hu_\alpha + k\,v_\alpha + lw_\alpha)}\,. \tag{3.47}$$

As an example we consider the body-centered cubic lattice. The two atoms in the unit cell occupy the positions

$$r_1 = (0,\,0,\,0) \quad \text{and} \quad r_2 = (1/2,\,1/2,\,1/2)\,.$$

Both have the same atomic scattering factor f.

For S it follows that

$$S_{hkl} = f(1 + \mathrm{e}^{-\mathrm{i}\,\pi(h+k+l)}) = \begin{cases} 0 & \text{for } h+k+l \quad \text{odd} \\ 2f & \text{for } h+k+l \quad \text{even} \end{cases}. \tag{3.48}$$

This lattice therefore gives rise to systematic extinctions. For example there is no (100) reflection. The (100) planes form the faces of the unit cell and the reason for the destructive interference is the presence of the additional intermediate lattice planes containing the atoms in the body-centered position (Fig. 2.10). A prerequisite for the complete extinction of the Bragg reflections is that the central atom is identical to the corner atoms, in other words, one must have a true body-centered Bravais lattice. The CsCl structure, for example, does not produce extinctions, except in the case of CsI where the electron numbers of Cs^+ and I^- are identical.

It is easy to show that other centered lattices also lead to systematic extinctions.

Even when the complete extinction produced by centered lattices is not observed, the intensities of the diffraction beams are nonetheless modulated by the presence of additional atoms within the unit cell. This fact enables one to determine the positions and types of atoms in the unit cell. We summarize by stressing an important point: the *shape* and the *dimensions* of the unit cell can be deduced from the position of the Bragg reflections; the *content* of the unit cell, on the other hand, must be determined from the intensities of the reflections.

3.7 Methods of Structure Analysis

Types of Probe Beam

For structure investigations one can employ electrons, neutrons, atoms and X-ray photons. In each case, the wavelength must lie in a region that allows Bragg reflections to be produced. It is this condition that determines the respective energy ranges of the beams (Fig. 3.11). These are

10 eV	–	1 keV	for electrons,
10 meV	–	1 eV	for neutrons and light atoms,
1 keV	–	100 keV	for photons.

The actual uses of these various probes in structure analyses are determined by the cross sections for elastic and inelastic scattering, and also by the availability and intensity of the sources.

For electrons between 10 eV and 1 keV the scattering cross sections are so large that only 10–50 Å of solid material can be penetrated by the beam. Thus electrons are frequently employed to gather information about the atomic structure of surfaces. Diffraction experiments with atoms offer a further method of investigating surfaces (Panel I).

In the case of photons, depending on the nature of the target material and the type of radiation, it is possible to investigate the bulk structure of targets up to several mm in thickness. As a source of radiation one generally employs the characteristic X-ray lines emitted by solids under electron bombardment (X-ray tubes). Such sources also produce a continuous brems-

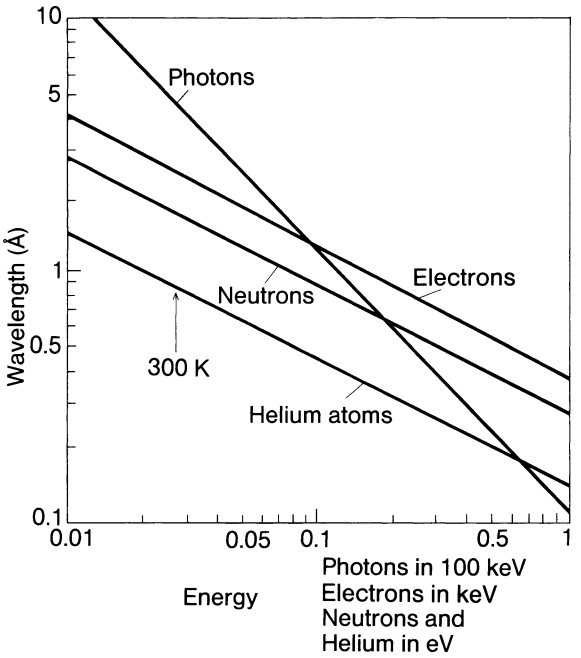

Fig. 3.11. The de Broglie wavelength of photons, electrons, neutrons and helium atoms as a function of the particle energies. The arrow shows the energy for a thermal beam at room temperature (eV scale)

strahlung spectrum. The spectrum of characteristic lines is caused by the ionization of atoms, which is followed by the emission of light when electrons from higher energy levels fall into the vacant state. Another excellent source of X-rays possessing high intensity and strongly collimated beams with 100% polarization is the electron synchrotron (e.g., "DESY" in Hamburg, "BESSY" in Berlin, ESRF in Grenoble, NSLS in Brookhaven, or ALS in Berkeley; see Panel V). Because of the ready availability of X-ray sources, the majority of structure investigations to date have been carried out with X-ray beams. However, there are a number of questions that cannot be answered with X-ray studies. We have seen that the atomic structure factors are proportional to the nuclear charge Z. Thus the scattering intensities vary as Z^2. Therefore, when hydrogen, for example, occurs in combination with heavy elements, it is very difficult to detect it with X-rays. Here it is better to use neutron beams. The scattering cross section for neutrons lies within a single order of magnitude for all elements. On the other hand, the neutron cross sections for elements with adjacent atomic numbers, which are difficult to distinguish with X-ray diffraction, are quite different. Hence it is possible, for example, to easily distinguish iron, cobalt and nickel in neutron scattering (Panel I). A difficulty with neutrons, however, is that intense beams can only be obtained from nuclear reactors or, more recently, also from so-called spallation sources. Furthermore,

the cross sections are small and the detection of the beams is less straightforward. Thus the necessary experimental effort is far greater than for X-ray or electron scattering. Neutron beams are utilized particularly in circumstances where one can take advantage of their specific properties, e.g., for investigating the structure of organic materials and polymers.

Procedures for Determining Structure

The incidence of a monochromatic plane wave on a crystal does not, in general, lead to any diffracted beams. We can see this immediately from the Ewald construction (Fig. 3.4). Only for particular choices of the wavelength (i.e. the magnitude of $\boldsymbol{k}_0$), or for particular angles of incidence, will a point of the reciprocal lattice fall on the Ewald sphere. The various procedures for determining structures differ in the method by which this condition is obtained. One can, for example, simply turn the crystal (preferably about a principal axis oriented perpendicular to the incident beam). Since the reciprocal lattice is associated in a fixed manner to the real crystal lattice, a rotation of the crystal corresponds to a rotation of the reciprocal lattice through the Ewald sphere (whose position in space is defined by the incident beam and is therefore fixed). One after another the points of the reciprocal lattice pass through the surface of the Ewald sphere. Thus, for particular rotation angles diffracted beams emerge in certain directions and these can be imaged by placing a photographic film around the crystal. This is the so-called rotating crystal procedure. To obtain an unambiguous indexing of the beams, the crystal is in addition translated along the axis of rotation (Weissenberg method). Together, these two procedures can be used to determine unknown crystal structures.

Using the powder method developed by Debye and Scherrer, it is possible to measure the lattice constant to an accuracy of five decimal places. In this technique the beam is directed at a powder composed of tiny single crystals whose random orientation ensures that all possible reflections are produced. In terms of the Ewald construction in reciprocal space (Fig. 3.4) one can determine the allowed reflections by imagining the reciprocal lattice to be rotated about the origin through the Ewald sphere. Since all orientations are present in the powder, a reflection is produced for every lattice point that passes through the sphere in the course of the rotation. In other words, one observes all reflections that lie within a radius of $2k_0$ from the origin of the reciprocal lattice. The powder method can be used, for example, to measure the change of lattice constant with temperature or with varying composition of an alloy.

The simplest method of producing diffraction is to use an incident beam containing a continuous spectrum of wavelengths, for example, the X-ray bremsstrahlung spectrum. In this case one observes all reflections whose lattice points lie between the Ewald spheres corresponding to the minimum and maximum k_0 values of the incident radiation.

This so-called Laue method has the advantage that, for a suitable orientation of the crystal, one can determine the crystal symmetry directly from the diffraction pattern. For instance, if the incident beam is directed along an n-fold symmetry axis, then the diffraction pattern also displays n-fold symmetry. Thus the Laue method is often used to determine the orientation of crystals of known structure and plays an important role in the preparation of crystals that are to be used as targets in other investigations. It cannot be applied, however, for the determination of structure.

Problems

3.1 a) Show that the reciprocal lattice of the reciprocal lattice is the original real-space lattice:
Hint: let $\boldsymbol{G} = m_1\boldsymbol{g}_1 + m_2\boldsymbol{g}_2 + m_3\boldsymbol{g}_3$ be reciprocal lattice vectors of the real-space lattice and the $\boldsymbol{g}_i$ the corresponding basis vectors. Then, by definition, the reciprocal lattice vectors of the reciprocal lattice $\boldsymbol{G}^* = n_1\boldsymbol{g}_1^* + n_2\boldsymbol{g}_2^* + n_3\boldsymbol{g}_3^*$ must satisfy $\boldsymbol{G}^* \cdot \boldsymbol{G} = 2\pi k$, where k is an integer. This is the case for $\boldsymbol{g}_1^* = 2\pi \dfrac{\boldsymbol{g}_2 \times \boldsymbol{g}_3}{\boldsymbol{g}_1 \cdot (\boldsymbol{g}_2 \times \boldsymbol{g}_3)}$ and for cyclic permutations of the indices.

b) Let the function $f(\boldsymbol{r})$ be lattice periodic. Show that the vectors $\boldsymbol{k}$ occurring in the Fourier series $f(\boldsymbol{r}) = \sum_k \hat{f}_k \exp(\mathrm{i}\boldsymbol{k} \cdot \boldsymbol{r})$ are reciprocal lattice vectors $\boldsymbol{G}$.

3.2 a) Calculate the structure factor $S_{hkl} = \sum_\alpha f_\alpha \exp(-\mathrm{i}\,\boldsymbol{G}_{hkl} \cdot \boldsymbol{r}_\alpha)$ for the face-centered cubic structure. For which indices hkl does one find extinction of the diffracted beams?

b) The fcc structure arises as the result of an appropriate superposition of four interpenetrating primitive simple cubic (sc) structures, all of which have the same lattice constant as the fcc structure. Interpret the result of part (a) for the case of the (001) diffraction beam (extinction compared with sc), and for the (111) beam (enhancement compared with sc). To do this, consider the Bragg reflection from the corresponding lattice planes of the sc and the fcc structures, making use of relevant sketches.

3.3 Calculate the structure factor for the diamond structure.

3.4 Show that the reciprocal lattice of a two-dimensional lattice can be represented by rods. Discuss the Ewald construction for diffraction from a two-dimensional lattice and determine the diffracted beam for a particular orientation and magnitude of $\boldsymbol{k}_0$. Why does one observe a diffraction pattern of electrons from a surface for all values and orientations of $\boldsymbol{k}_0$ above a critical value? Calculate the critical energy at which the first diffracted beam appears, when the electrons are incident perpendicular to a (100) surface of a Cu crystal.

3.5 Calculate the diffraction intensities from a rectangular lattice formed by the lattice vector $\boldsymbol{r_n} = 2an\boldsymbol{e}_x + am\boldsymbol{e}_y$ with a basis of atoms at (0, 0) and ($\frac{1}{2}$, ϱ). Where do you find (glide plane) extinctions? Discuss the result with regard to the dependence on ϱ.

3.6 Consider the matrix element for the absorption of an X-ray photon by an atom $\langle i|x|f\rangle$ where $\langle i|$ is the initial localized state of an electron residing on the atom and $\langle f|$ is the final s-wave $\Psi = \mathrm{e}^{\mathrm{i}kr}/r$ with $\hbar^2 k^2/2m = \hbar\nu - E_\mathrm{I}$, where E_I is the threshold energy for ionization. Now assume that the atom is surrounded by a shell of nearest neighbor atoms that scatter the emitted wave. The final state thus consists of the emitted spherical wave plus spherical waves scattered from the ensemble of nearest neighbor atoms. What do you expect for the X-ray absorption above threshold? Describe a method to determine the distance of nearest neighbors in an amorphous material from the oscillations in the absorption coefficient of X-rays above threshold (**E**xtended **X**-ray **A**bsorption **F**ine **S**tructure: EXAFS). What type of light source is needed? Why does the method require the investigation of the oscillatory structure at photon energies considerably above the threshold? Why is it (experimentally) difficult to determine the local environment of carbon in an amorphous matrix?

3.7 a) Show that the contribution of large r to the correlation function $g(r)$ (3.14) leads to forward scattering! How can one determine the correlation function $g(r)$ from the experimentally observed intensity $I(\boldsymbol{K})$ even when the intensity of the forward scattering $I(\boldsymbol{K} = \boldsymbol{0})$ is not known?

b) Liquids are characterized by vanishing shear forces. By virtue of the Pauli-principle atoms behave nearly as hard spheres. Demonstrate with the help of hard spheres (e.g. tennis balls) that the distance of next nearest neighbors in liquids must be on the average at least $2r\sqrt{3}$ with r the radius of the spheres, or half the distance to the next neighbors. Compare this result to Fig. 3.2! Why do these considerations not apply to water?

3.8 Calculate the scattered intensity from a linear chain of atoms with ordered domains of N atoms. Assume that there is no phase correlation between atoms in different domains.

3.9 Discuss qualitatively the atomic scattering factor (as a function of scattering angle) for electron, X-ray, and neutron diffraction by a crystalline solid.

3.10 Elastic scattering by an infinite periodic crystal lattice yields infinitely sharp Bragg reflection spots according to (3.26). Discuss, on the basis of the Fourier transform representation of the scattered intensity (3.26), diffraction from crystallites of finite size. How can the average size of a crystallite be estimated from the diffraction pattern?

Panel I
Diffraction Experiments with Various Particles

I.1 Electrons

We describe here an experiment in which low energy (10–1000 eV) electrons are diffracted (LEED – Low Energy Electron Diffraction). In solids, low energy electrons are absorbed before they have penetrated more than a few atomic lattice planes. Thus diffraction experiments can only be performed in a reflection mode and they deliver information about the structure of the topmost atomic layers of a crystal. The first electron diffraction experiment was carried out by Davisson and Germer [I.1] in 1927, and served to demonstrate the wave nature of electrons. An experimental arrangement that conveniently enables the diffraction beams to be imaged on a fluorescent screen is shown in Fig. I.1. Because of the surface sensitivity of the method, it is necessary to perform LEED experiments in ultra-high vacuum ($p < 10^{-8}$ Pa) and on atomically "clean" surfaces. An example showing the diffraction pattern obtained from a (111) surface of nickel is given in

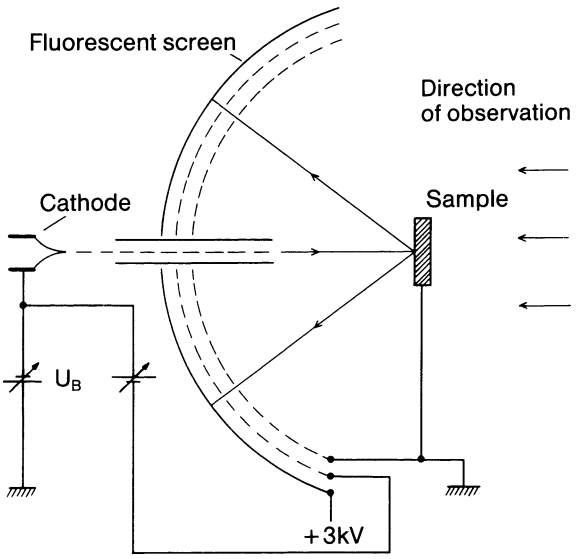

Fig. I.1. Schematic of the experimental arrangement used to observe LEED reflections from the surface of a single crystal

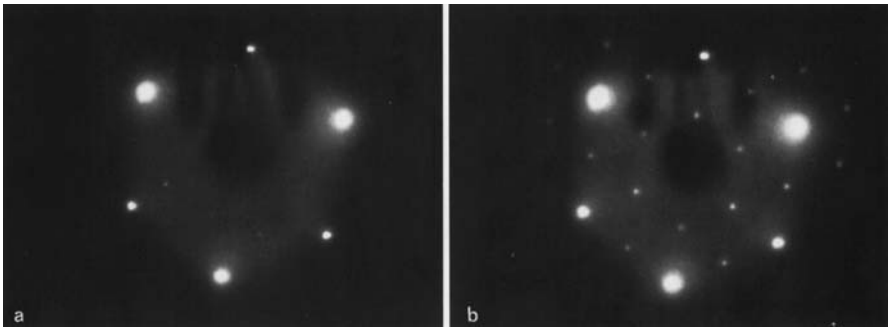

Fig. I.2. (**a**) LEED diffraction pattern from a Ni (111) surface at a primary electron energy of 205 eV, corresponding to a wavelength of 0.86 Å. The position of the spots can be used to determine the lattice constant. Of perhaps greater interest are adsorption experiments since adsorbates often form a variety of overlayer structures. (**b**) The diffraction pattern observed after the adsorption of hydrogen. The extra spots indicate the formation of a so-called (2×2) adsorbate superstructure, i.e., the elementary mesh of the adsorbate structure is, in both directions, twice as large as that of the nickel substrate

Fig. I.2. The strong absorption of the electrons means that the third Laue condition for the constructive interference between electrons scattered from the atomic planes parallel to the surface is of little importance. As a result it is possible to observe diffraction at all electron energies. It should be noted that the diffraction pattern of Ni(111) displays the true 3-fold symmetry of the body of an fcc crystal since the scattering is not only from the surface layer but includes contributions from deeper layers. Figure I.2 b shows the diffraction pattern of the same surface after the adsorption of hydrogen. The additional diffraction spots indicate that the hydrogen – like many other adsorbates on surfaces – creates an overlayer with a new structure. In this case the elementary mesh of the hydrogen overlayer is exactly twice the size of that of the Ni(111) surface. The additional spots therefore lie halfway between those of the nickel substrate.

I.2 Atomic Beams

The diffraction of He and H_2 beams from solid surfaces was first detected in the experiments of Estermann and Stern [I.2]. At the time, this result provided vital confirmation of the validity of quantum mechanics! From a modern viewpoint it must be judged a very lucky chance that Estermann and Stern chose to work with alkali halide crystals (NaCl and LiF). Indeed most other surfaces, especially those of metals would not have led to the observation of the diffraction phenomenon. The reason is that He atoms with an appropriate wavelength (Fig. 3.11) only interact with the outermost surface of the solid where the interaction potential is very smooth and thus they are hardly sensitive to the atomic structure of the crystal. Furthermore,

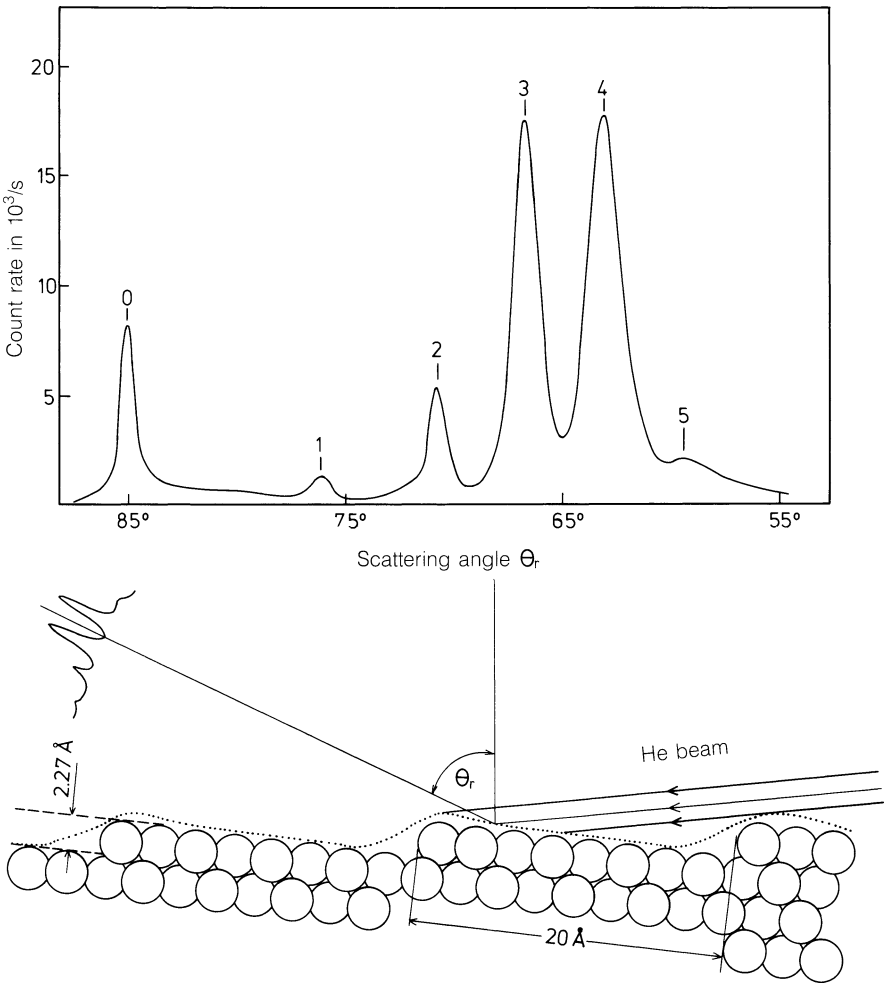

Fig. I.3. Diffraction of a He beam from a stepped platinum surface [I.3]. The Miller indices of this surface are (997). As for an optical echelon, one obtains maximum intensity in the diffraction orders that correspond to specular reflection from the contours of the interaction potential. In this case it should be noted that these potential contours are not exactly parallel to the terraces

diffraction experiments on metals and most other materials could never have been successful prior to the development of ultra-high vacuum technology, which today allows us to prepare extremely clean surfaces.

We show here as an example the diffraction of He atoms from a stepped platinum surface (Fig. I.3) as measured by Comsa et al. [I.3]. Surfaces with regularly spaced monatomic steps can be produced by cutting the crystal at the appropriate angle and annealing in vacuum. The atomic beam used in the diffraction experiments is produced by a supersonic expansion of the gas

from a nozzle. The interaction between the atoms in the expanding gas produces a velocity distribution that is significantly sharper than the Maxwell distribution present before the expansion. Here one can make an analogy to vehicles traveling on a crowded freeway that have to adjust their forwards velocity to that of the other vehicles.

In Fig. I.3 the diffracted intensity is shown as a function of scattering angle. The angle of incidence is 85° to the surface normal of the macroscopic surface. The intensity maxima correspond to the diffraction orders of the periodic lattice of terraces (and not the lattice of individual atoms!). As is the case for an optical echelon grating, the direction corresponding to specular (mirror) reflection from the terraces is favored in the intensity distribution. Here, however, there is a slight bump in the otherwise flat potential of the terraces near to the step edge. This leads to a slight shift in the intensity maximum towards smaller angles.

I.3 Neutrons

The first diffraction experiments with neutrons were carried out as long ago as the 1930s. However, only since about 1945, when high neutron fluxes became available with the advent of nuclear reactors, has it been possible to employ neutron beams for structure investigations. The majority of the neutrons produced are so-called thermal neutrons ($T \sim 400$ K). As can be seen from Fig. 3.11, the de Broglie wavelength then falls in a favorable range for atomic structure studies. Two methods are commonly used to obtain neutrons of a defined de Broglie wavelength. The crystal monochromator exploits the wavelength dependence of the Bragg-reflection. Monochromaticity is achieved by selecting a small range of reflection angles. Alternatively, time-of-flight-spectrometers are used. A sequence of at least two rotating slits selects neutrons of a particular velocity, hence a particular de Broglie wavelength. Today more and more pulsed neutron sources (*spallation sources*) become available. In that case, the total white spectrum of a pulse can be used for structure analysis as in the Laue-method. Contrary to the classical Laue-method however, the velocity and hence the wavelength of the scattered neutron can be determined afterwards by measuring the time of flight between the sample and the neutron detector. A particular Bragg reflex is thereby attributed to the particular wavelength that generated the reflection, as is required for structure analysis.

The most important applications of neutron diffraction are the determination of the location of hydrogen atoms in solids and biological systems, the investigation of magnetic structures, and the study of order-disorder phase transitions [I.4]. We will discuss an example from the field of phase transitions. The alloy FeCo composed of an equal number of Fe and Co atoms crystallizes in the bcc structure. At high temperatures and for rapidly

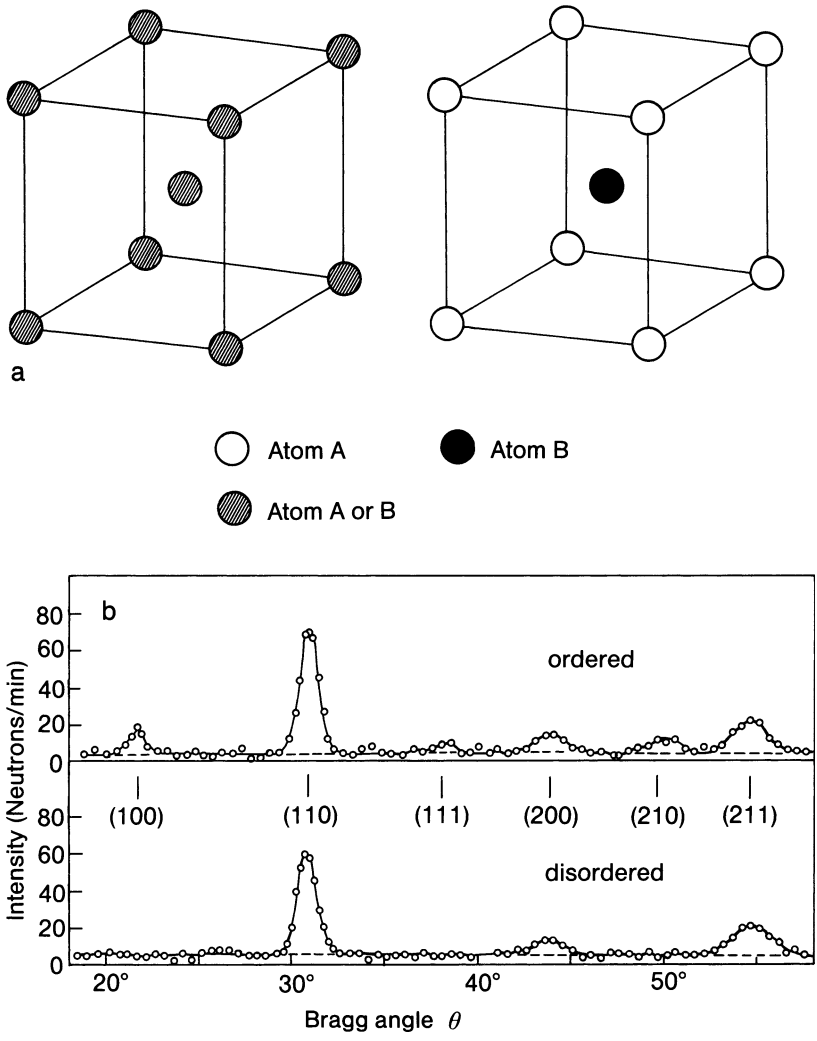

Fig. I.4. (**a**) The disordered and ordered phases of FeCo. (**b**) Neutron diffractogram of the ordered and disordered phases; after [I.5]. Note the low count rates which are typical for neutron diffraction experiments. To obtain good statistics it is necessary to measure for long periods of time

quenched samples, the Fe and Co atoms are distributed randomly among the sites of the bcc lattice (Fig. I.4a). If, however, the crystal is cooled slowly, an ordered phase is produced in which the corner and body-center positions are each occupied by only one of the two elements. This arrangement corresponds to a CsCl lattice. Similar ordering phenomena are also found for other alloy systems and also include other lattice types. They can be detected and studied by means of diffraction experiments.

In Sect. 3.6 we met the systematic extinctions of the face-centered cubic lattice. These extinctions affect all diffraction beams for which the sum $h+k+l$ is odd, i.e., the (100), (111), (210) etc. For this disordered alloy phase (Fig. I.4a, left) these beams are thus absent. For the ordered phase, however (Fig. I.4a, right), the beams are present since the atomic scattering factors of Fe and Co are not equal. In principle, this behavior is to be expected for every type of radiation. For X-rays, however, the atomic scattering factors of Fe and Co only differ slightly since the two elements are neighbors in the periodic table and since the atomic scattering factor for X-rays varies systematically approximately in proportion to the nuclear charge Z. As is readily seen from (3.47), the intensity of the (100) reflection of the CsCl structure (ordered phase) is proportional to $(f_{\mathrm{Fe}} - f_{\mathrm{Co}})^2$. The degree of order in the alloy is thus generally hard to determine from X-ray diffraction. Quite different is the case of neutron scattering: Here there is a factor 2.5 difference between the atomic scattering factors of Fe and Co. Figure I.4b shows neutron diffraction scans from powders of ordered and disordered FeCo. The forbidden reflections in the bcc structure, (100), (111), (210), are clearly visible for the ordered phase with the CsCl structure.

References

I.1 C.J. Davisson, L.H. Germer: Nature 119, 558 (1927); Phys. Rev. 30, 705 (1927)
I.2 I. Estermann, O. Stern: Z. Phys. 61, 95 (1930)
I.3 G. Comsa, G. Mechtersheimer, B. Poelsema, S. Tomoda: Surface Sci. 89, 123 (1979)
I.4 G.F. Bacon: Neutron Diffraction, 2nd edn. (Oxford Univ. Press, Oxford 1962)
I.5 C.G. Shull, S. Siegel: Phys. Rev. 75, 1008 (1949)

Panel II
X-Ray Interferometry and X-Ray Topography

X-ray beams may be used not only to determine the structural parameters of single crystals, but also to determine deviations from periodic structure and to observe defects in the structure. With X-ray interferometry it is possible, for example, to image even slight strains within a crystal.

As is well known, interference phenomena can be observed in the superposition of waves of equal frequency and with a fixed phase relation to one another. In optics, this is achieved by the division and subsequent recombination of a light beam. It is possible to proceed analogously with X-rays. To do so one makes use of an arrangement such as that shown in Fig. II.1. The blocks labeled S, M and A represent perfect single crystals that are aligned exactly parallel to one another. In the scatterer S a suitable incident angle gives rise to Bragg reflection from the lattice planes. As described in Sects. 3.4 and 7.2, two types of waves are induced in the crystal, one which has intensity nodes at the atomic sites, and a second for which the nodes lie between the atoms (see also Fig. 7.4). For large crystals, only the first type of wave survives, whereas the second is strongly absorbed (anomalous

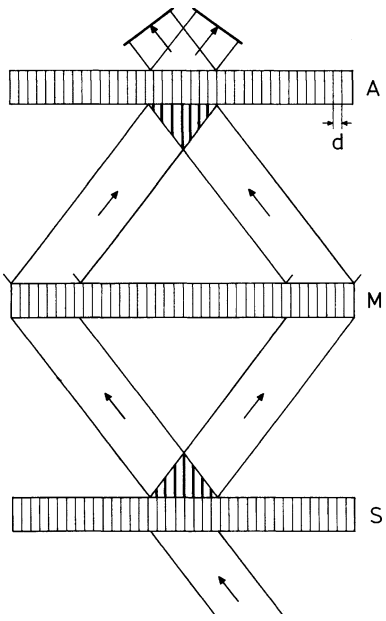

Fig. II.1. An arrangement for measuring X-ray interference [II.1]. The length d (not to scale!) represents the separation of lattice planes

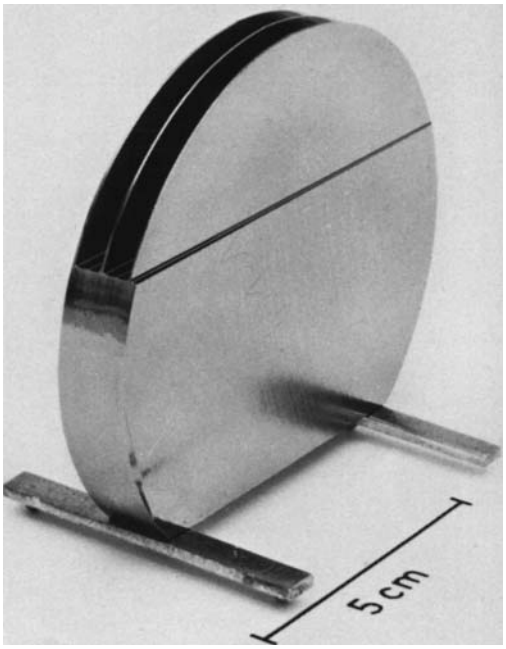

Fig. II.2. An X-ray interferometer made from a single crystal silicon disk

Fig. II.3. Moiré topography of the silicon interferometer. The vertical lines are due to the fact that the pattern is recorded in strips

transmission and absorption). What emerges from the crystal are two beams of equal intensity, one being the transmitted beam and the other the Bragg reflected beam. These beams are recombined by means of a further Bragg reflection at the "mirror" M. The nodes and antinodes of the standing wave have the same positions here as in the scattering crystal. If the lattice planes in the analyser A have the same position relative to the nodes as those in S, then the beams are transmitted by A and we observe brightness. If, however, the analyser A is displaced by half a lattice constant the wave is strongly absorbed and we observe darkness. When the lattices of S and A are not identical this gives rise to a Moiré pattern.

Figures II.2 and 3 illustrate an example taken from Bonse by [II.1]. The interferometer (Fig. II.2) is carved from a single silicon crystal of diameter 8 cm. The corresponding Moiré topograph (Fig. II.3) indicates that the crystal contains extended distortions.

The alternating bright and dark conditions that are obtained when A is gradually displaced relative to S (Fig. II.1) can also be used to provide a direct determination of the lattice constant. One simply needs to divide the total mechanical displacement by the number of bright/dark phases observed and thereby obtains the lattice constant without needing to know the wavelength of the X-rays. This procedure can be used to achieve an exact relation between the X-ray wavelength scale and the definition of the meter by way of the red emission line of ^{86}Kr. Whereas X-ray interferometry produces

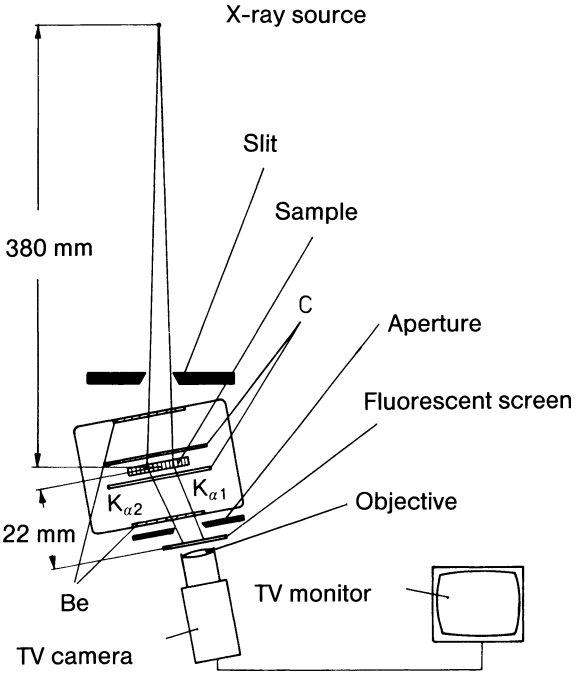

Fig. II.4. X-ray topography for the direct imaging of lattice defects [II.3]. The crystal is situated in an oven with beryllium windows. Beryllium, on account of its small nuclear charge, displays only weak X-ray absorption. The oven can be heated by means of graphite rods. Lattice defects appear as bright patches on the fluorescent screen and their development in time can be followed using a TV monitor

a Moiré pattern of lattice strain and defects, X-ray topography further enables one to make direct obervations. We consider here the experimental arrangement of Hartmann [II.2] (Fig. II.4). The X-rays from a Mo-K_α source are incident on a crystal and after being Bragg reflected are made visible on a fluorescent screen. For an ideal point source, only the two beams illustrated in Fig. II.4 would satisfy the Bragg condition. For a source of finite extent, however, one obtains bright patches on the screen. By a suitable choice of the size of the source these patches can be made sufficiently large that the areas of illumination of $K_{\alpha 1}$ and $K_{\alpha 2}$ just overlap. For fixed wavelengths of the radiation, this arrangement implies that a single point on the screen corresponds to a single point of the source. If, however, the crystal contains imperfections, then the Bragg condition for a point on the screen is satisfied not for a single point on the source, but for a large area or even for the entire source. Thus crystal imperfections lead to additional brightness on the screen. Figure II.5a illustrates this for the case of a silicon crystal upon which an indentation has been made

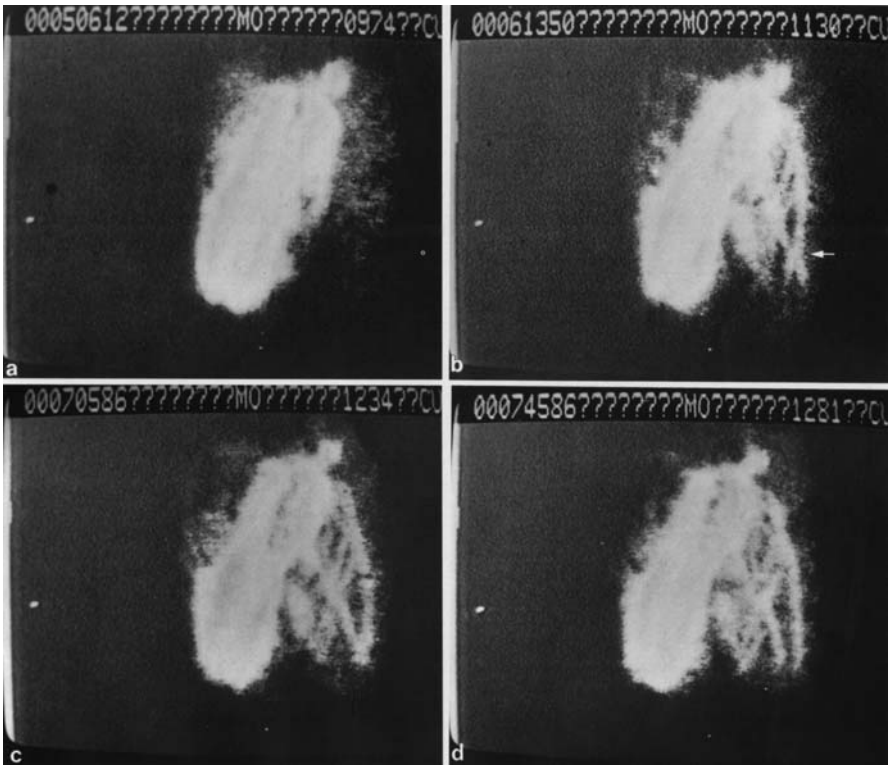

Fig. II.5. (a) X-ray topograph of a silicon crystal damaged by pressure from a diamond [II.3]. (**b**) After annealing at 1130 °C the formation of dislocations is observed. Two dislocations (*arrow*) have an intersection. (**c**) The intersection has wandered to the surface. The temperature is now 1234 °C. (**d**) The dislocations have separated and continue to move away from one another

with a diamond. At high temperatures it is possible for lattice defects to be partially repaired. Dislocations, however, remain in the crystal. A schematic representation of a dislocation is shown in Fig. 2.20. A dislocation gives rise to a strain field along a line and this, too, can be imaged by topography. Figure II.5b shows such dislocation lines produced after annealing of the silicon crystal. At even higher temperatures the dislocations become mobile and move away from one another (Fig. II.5c).

References

II.1 U. Bonse, W. Graeff, G. Materlik: Rev. Phys. Appl. 11, 83 (1976);
U. Bonse: Private communication (1979)
II.2 W. Hartmann: In *X-Ray Optics*, ed. by H.J. Queisser, Topics Appl. Phys. Vol. 22 (Springer, Berlin, Heidelberg 1977) p. 191
II.3 W. Hartmann: Private communication